absorption, i.e., −0.1 V, in the ethanol solution was consistent with that in the methanol solution. In the case of 2% H_2O, the corrosion potential gradually shifted to the noble direction and reached 0.3 V. As shown in Fig. 9(a) and (b), slight corrosion was observed on the surface of the specimen immersed in ethanol solution with 2% H_2O after 120 h, although mass loss and increment in the amount of desorbed hydrogen were rarely detected. In a separate experiment, we have confirmed that when the specimen is immersed in 0.07% HCl-containing ethanol solution with 0.6% H_2O for 120 h, hydrogen absorption always occurs: the amount of absorbed hydrogen does not scatter (98 ± 7 mass ppm, $n = 5$). These results suggest that the minimum critical H_2O concentration in 0.1% HCl-containing ethanol solution needed to inhibit hydrogen absorption is approximately 0.8%. It is likely that the hydrogen absorption of the Ni–Ti superelastic alloy immersed in the ethanol solution is more susceptible to the H_2O concentration in comparison with that in the methanol solution. Furthermore, the H_2O concentration in the ethanol solution is probably one origin of the scattering of hydrogen absorption reported previously [2].

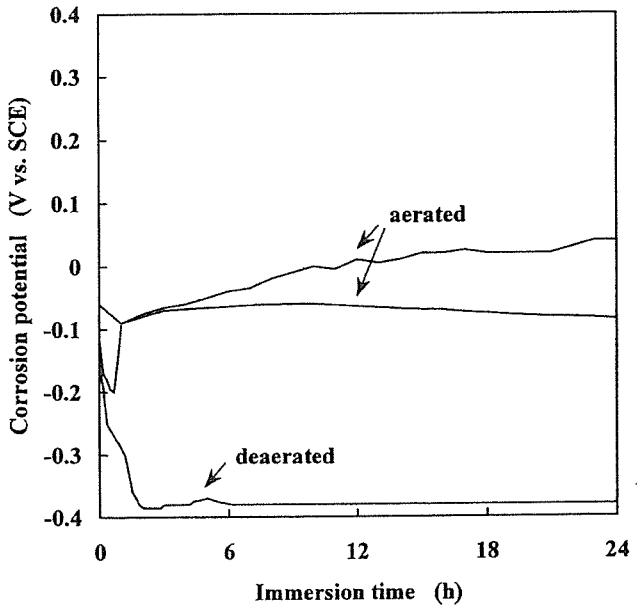

Fig. 10. Changes in corrosion potentials of specimens in ethanol solution under aerated and deaerated conditions.

3.4. Effects of dissolved oxygen in ethanol solution

As shown in Fig. 10, the corrosion potential of the Ni–Ti superelastic alloy was stabilized at approximately −0.38 V without scattering in the 0.1% HCl-containing ethanol solution with 0.8% H_2O under the deaerated condition. The side surfaces of the specimens immersed in the ethanol solution for 24 h under aerated and deaerated conditions are shown in Fig. 11. Under the aerated condition, very slight corrosion was observed (Fig. 11(a) and (b)), whereas under the deaerated condition, general corrosion was observed (Fig. 11(c) and (d)). The corrosion of titanium and its alloys does not always occur in the low-dissolved-oxygen conditions in solutions. For instance, in ethanol solution containing NaCl [5] or in artificial saliva [27], the corrosion resistance of titanium and its alloys does not differ much between aerated and deaerated conditions. Nonetheless, the present results show that the absence of dissolved oxygen markedly reduces the corrosion resistance of the Ni–Ti superelastic alloy in the ethanol solution.

Hydrogen thermal desorption curves from specimens immersed in the 0.1% HCl-containing ethanol solution with 0.8% H_2O after 24 h under aerated and deaerated conditions

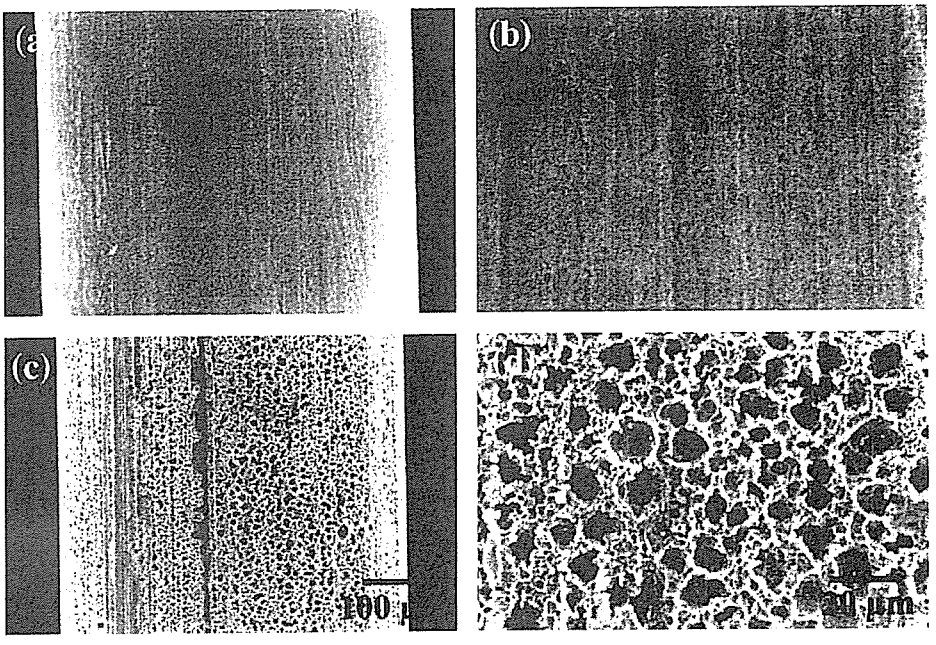

Fig. 11. SEM images of typical side surface: (a) general and (b) magnified views of specimen immersed in ethanol solution 24 h under aerated condition; and (c) general and (d) magnified views of specimen immersed in ethanol solution for 24 h under deaerated condition.

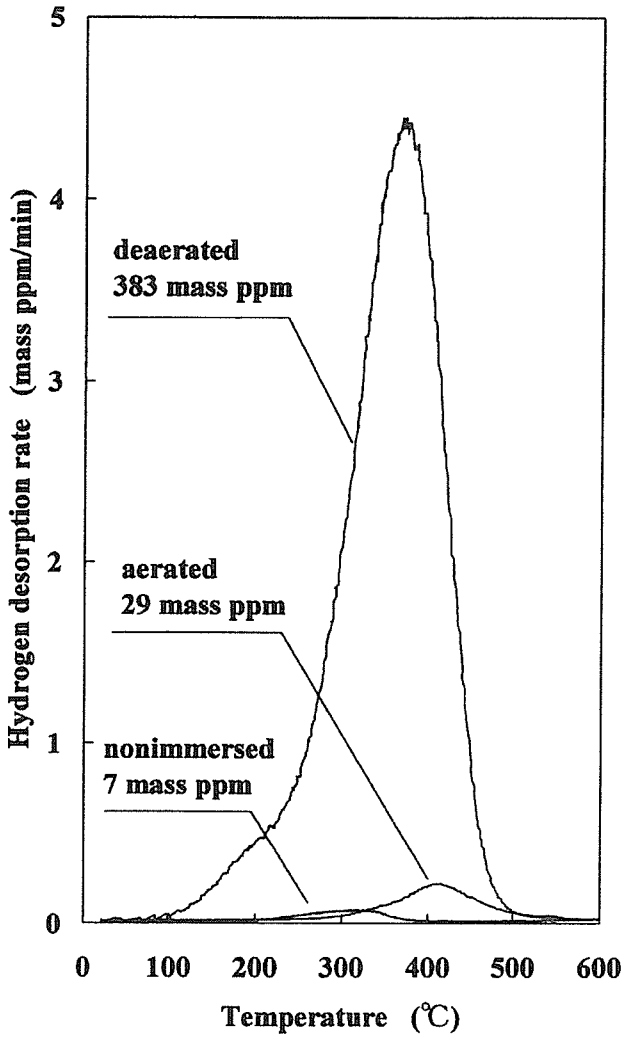

Fig. 12. Hydrogen thermal desorption curves obtained from specimens immersed in ethanol solution for 24 h under aerated and deaerated conditions.

are shown in Fig. 12. Under the deaerated condition, hydrogen absorption always occurred and hydrogen desorption peak appeared at approximately 380 °C. Under the aerated condition, hydrogen desorption peak appeared at approximately 420 °C; however, as the amount of absorbed hydrogen increased, the hydrogen desorption was observed as two peaks at approximately 150 and 350 °C [2]. That is, for the same amount of absorbed hydrogen, the hydrogen desorption behavior differs between aerated and deaerated conditions.

The amount of desorbed hydrogen under the deaerated condition (383 mass ppm) was one order of magnitude larger that under the aerated condition (29 mass ppm). The hydrogen absorption rate, i.e., the amount of absorbed hydrogen per unit time, was extremely enhanced by the absence of dissolved oxygen. The hydrogen absorption rate might affect the hydrogen desorption behavior. Thus, it seems that the absence of dissolved oxygen leads to the increment in the hydrogen absorption rate, thereby changing the hydrogen desorption behavior. However, even if the hydrogen absorption rate is the same, the hydrogen desorption behavior is not necessarily the same [1,2,25,28–30]. Accordingly, the change of the hydrogen desorption behavior may be ascribed to effects of dissolved oxygen itself. In any case, dissolved oxygen changes the hydrogen desorption behavior, namely, the state of hydrogen or trap sites in the Ni–Ti superelastic alloy.

In the ethanol solutions both under aerated and deaerated conditions, hydride formation was not confirmed by XRD measurements. Moreover, from desorbing hydrogen at high temperature, most of the hydrogen absorbed under the deaerated condition is perhaps trapped strongly. The state of hydrogen or trap sites is still being analyzed.

In the present study, it became clear that as causes of changes of the hydrogen absorption and desorption behaviors of the Ni–Ti superelastic alloy immersed in methanol and ethanol solutions containing 0.1% HCl, there are effects of the H_2O concentration and dissolved oxygen. Haruna et al. [31] demonstrated that initiation of environment-assisted cracking of titanium in methanol solution containing $CaCl_2$ is dominated by the concentration of dissociated chloride ion. Usually, HCl is easily dissociated into hydrogen and chloride ions in methanol solution, compared with ethanol solution. This difference of the dissociation behavior of HCl also may affect hydrogen absorption and desorption behaviors.

4. Conclusions

We have demonstrated that H_2O concentration and dissolved oxygen in methanol and ethanol solutions containing 0.1% HCl affect hydrogen absorption and desorption behaviors of the Ni–Ti superelastic alloy. In the methanol solution, for 5% H_2O, the thermal desorption peak shifts to the low-temperature region. Upon adding 10% H_2O to the solution, hydrogen absorption is suppressed. The absence of dissolved oxygen results in the dissolution of the specimen being faster than hydrogen entry into the specimen. In the ethanol solution, the H_2O concentration for the inhibition of hydrogen absorption is above 0.8%. The absence of dissolved oxygen enhances extremely the hydrogen absorption rate and changes the hydrogen thermal desorption to a single peak at approximately 380 °C.

Acknowledgements

This study was supported in part by a Grant-in-Aid for Young Scientists (B) (17791397) and a Grant-in-Aid for Scientific Research (C) (15560632) from the Ministry of Education, Culture, Sports, Science and Technology, Japan.

References

[1] K. Yokoyama, T. Ogawa, K. Asaoka, J. Sakai, M. Nagumo, Mater. Sci. Eng. A 360 (2003) 153.
[2] T. Ogawa, K. Yokoyama, K. Asaoka, J. Sakai, Mater. Sci. Eng. A 393 (2005) 239.
[3] K. Mori, A. Takamura, T. Shimose, Corrosion 22 (1966) 29.
[4] G. Sanderson, J.C. Scully, Corros. Sci. 8 (1968) 541.
[5] A. Cerquetti, F. Mazza, Corros. Sci. 13 (1973) 337.
[6] A.C. Hollis, J.C. Scully, Corros. Sci. 34 (1993) 837.
[7] T. Haruna, M. Yamamoto, T. Shibata, J. Jpn. Inst. Met. 63 (1999) 977.

[8] W.Y. Choo, J.Y. Lee, Metall. Trans. A 13A (1982) 135.
[9] K. Ono, M. Meshii, Acta Metall. Mater. 40 (1992) 1357.
[10] A. Takasaki, Y. Furuya, K. Ojima, Y. Taneda, J. Alloys Compd. 224 (1995) 269.
[11] A. Turnbull, R.B. Hutchings, D.H. Ferriss, Mater. Sci. Eng. A 238 (1997) 317.
[12] S.W. Smith, J.R. Scully, Metall. Mater. Trans. A 31A (2000) 179.
[13] M. Nagumo, M. Nakamura, K. Takai, Metall. Mater. Trans. A 32A (2001) 339.
[14] K. Takai, R. Watanuki, ISIJ Int. 43 (2003) 520.
[15] T. Nishiue, Y. Kaneno, H. Inoue, T. Takasugi, J. Alloys Compd. 364 (2004) 214.
[16] I.A. Menzies, A.F. Averill, Electrochim. Acta 13 (1968) 807.
[17] J.C. Scully, T.A. Adepoju, Corros. Sci. 17 (1977) 789.
[18] K. Ebtehaj, D. Hardie, R.N. Parkins, Corros. Sci. 25 (1985) 415.
[19] T. Ogawa, K. Yokoyama, K. Asaoka, J. Sakai, J. Alloys Compd. 396 (2005) 269.
[20] N. Wade, Y. Adachi, Y. Hosoi, Scripta Metall. Mater. 24 (1990) 1051.
[21] T. Hoshiya, S. Den, H. Katsuta, H. Ando, J. Jpn. Inst. Met. 56 (1992) 747.
[22] T. Asaoka, T. Kamimura, H. Saito, Y. Ishida, J. Jpn. Inst. Met. 56 (1992) 1111.
[23] F.T. Cheng, P. Shi, H.C. Man, Scripta Mater. 47 (2002) 89.
[24] T. Ohba, F. Yanagita, M. Mitsuka, T. Hara, K. Kato, Mater. Trans. 43 (2002) 798.
[25] K. Yokoyama, K. Kaneko, K. Moriyama, K. Asaoka, J. Sakai, M. Nagumo, J. Biomed. Mater. Res. 69A (2004) 105.
[26] R. Schmidt, M. Schlereth, H. Wipf, W. Assmus, M. Müllner, J. Phys. Condens. Matter. 1 (1989) 2473.
[27] M. Nakagawa, S. Matsuya, K. Udoh, Dent. Mater. J. 21 (2002) 83.
[28] K. Yokoyama, S. Watabe, K. Hamada, J. Sakai, K. Asaoka, M. Nagumo, Mater. Sci. Eng. A 341 (2003) 91.
[29] K. Yokoyama, K. Kaneko, K. Moriyama, K. Asaoka, J. Sakai, M. Nagumo, J. Biomed. Mater. Res. 65A (2003) 182.
[30] K. Yokoyama, K. Kaneko, T. Ogawa, K. Moriyama, K. Asaoka, J. Sakai, Biomaterials 26 (2005) 101.
[31] T. Haruna, M. Yamamoto, T. Shibata, J. Jpn. Inst. Met. 63 (1999) 1327.

Bio-Medical Materials and Engineering 16 (2006) 83–91
IOS Press

Chemical surface modification of high-strength porous Ti compacts by spark plasma sintering

Yuki Sakamoto [a], Kenzo Asaoka [b,*], Masayuki Kon [b], Toshio Matsubara [c] and Kenichi Yoshida [a]

[a] *Department of Mechanical Engineering, Faculty of Engineering, The University of Tokushima, 2-1 Minamijosanjima-cho, Tokushima 770-8506, Japan*

[b] *Department of Biomaterials and Bioengineering, Institute of Health Biosciences, The University of Tokushima Graduate School, 3-18-15 Kuramoto-cho, Tokushima 770-8504, Japan*

[c] *Division of Electronics/Machinery, Tokushima Prefectural Industrial Technology Center, 11-2 Nishibari Saika-cho, Tokushima 770-8021, Japan*

Received 2 February 2005

Abstract. The biological properties of a titanium (Ti) implant depend on its surface oxide film. The aims of the present study were to increase the specific surface oxide area on Ti using a porous structure and to study the relationship between the amount of apatite coating in simulated body fluid (SBF) and the actual surface area on titanium powders. Ti powders of 110 μm average diameter were sintered by spark plasma sintering. The sintered compacts had a porosity of 28%, a compressive elastic modulus of 7.9 GPa and an ultimate strength of 112 MPa. The compressive strength of the compacts was increased to 588 MPa by subsequent annealing in a vacuum furnace at 1000°C for 24 h. The sintered compacts were treated with aqueous NaOH solution and subsequently heated at 600°C. The pretreated compacts showed apatite crystal precipitation in SBF. The amounts of precipitates through the compacts were compared with those of the Ti plate substrates subjected to the same chemical pretreatment. It was confirmed that the amounts of precipitates through the compacts were more than one hundred times higher than those on the Ti plates. It was concluded that the metal porous compacts developed may be used as functional materials for immobilizing functional proteins and/or drugs, because the precipitated apatite can adsorbed these substances.

Keywords: Titanium, porosity, mechanical properties, metal surface treatment, SBF (simulated body fluids)

1. Introduction

Medical devices such as artificial bones, joints, bone plates and nails in orthopedics, and dental implants need to have the following excellent properties, that is, biocompatibility and bio-adhesion, and mechanical properties similar to those of a metal. For these artificial biomaterials, titanium (Ti) and its alloys have been developed and used in modern clinics [1]. The mechanical properties of Ti strongly

*Corresponding author: Kenzo Asaoka, PhD, Department of Biomaterials and Bioengineering, Institute of Health Biosciences, The University of Tokushima Graduate School, 3-18-15 Kuramoto-cho, Tokushima 770-8504, Japan. Tel.: +81 88 633-7333; Fax: +81 88 633-9125; E-mail: asaoka@dent.tokushima-u.ac.jp.

0959-2989/06/$17.00 © 2006 – IOS Press and the authors. All rights reserved

depend on its heating and machining process [2]. The effective use of passive surface TiO_2 films depends on their chemical and electrochemical properties, which directly affect the biocompatibility of such alloys [3]. The microstructure and passive films related to the composition and metal process have been studied from the viewpoint of the biocompatibility.

Biocompatibility, which is defined as the ability of a biomaterial to demonstrate host and material response appropriate to its intended application, are basically classified into biological compatibility and mechanical compatibility [4]. In terms of biological compatibility, some types of calcium phosphate are superior in bone conduction to Ti and its alloys. From this, coatings of hydroxyapatite (apatite) on Ti substrates have been used as bone substitute biomaterials. Physical processes such as plasma spray coating, micro-arc oxidation and YAG laser deposition, electrochemical treatments such as anode oxidation, and the sol-gel method have been used in apatite coating [5–11]. However, chemical treatment using simulated body fluid (SBF) is an easy process for modification [12–15], and can be used to immobilize proteins/drugs onto a Ti substrate with an apatite layer [16,17].

Mechanical biocompatibility have been studied from the following view points, that is, improvement in mechanical properties such as strength, and elongation by Ti alloying, and development of low-elastic-modulus materials by Ti alloying [18] and use of porous compacts [19,20], because strain mismatch at the tissue–material interface under loading is related to elastic modulus. Bone growth into pores of materials is expected [21], when porous surface materials are used as implants. Many types of porous/foam Ti compacts have been developed [22]. Spark plasma sintering (SPS), which is an advanced sintering process using electric current, is expected to be feasible for developing porous Ti biomaterials [23–25].

When porous Ti compacts with excellent mechanical properties are developed, medical devices with biological and mechanical biocompatibility might concurrently be realized. A wide specific area of TiO_2 on Ti powders introduces many apatite crystals, if proper chemical pretreatment is performed. Such compacts can control their elastic modulus by their porosity, and then a low elastic modulus close to that of human cortical bone can be easily realized. In this study, Ti powders were sintered by SPS, and tested of their mechanical properties. The compacts were treated with aqueous NaOH solution and subsequently heat-treated. The chemically pretreated compacts were immersed in SBF, and measured of their mass changes due to precipitated apatite crystals on Ti powders. The amount of precipitates was compared with that of the Ti substrate, which had been treated by the same chemical pretreatment and immersion test.

2. Materials and methods

2.1. Specimen preparation

Spherical chemical pure Ti powders with diameter of less than 150 μm (Sumitomo Titanium Co. Amagasaki, Japan) were sieved using a 100-μm screen, and used as starting materials. The average diameter of the powders was 110 μm. The impurity atoms of the pure Ti powders was O, 0.099%; Fe, 0.033%; N, 0.029%; H, 0.009%; and C, 0.008% according to the manufacture and had been determined by chemical analysis. The powders were weighed to 0.01 g accuracy, and packed in a carbon die to cylindrical shape (5 mm $\varnothing \times$ 10 mm). The compressed powders were sintered using the SPS system (SPS-511S, Sumitomo Heavy Industries Ltd., Niihama, Japan), and 10 specimens were sintered by the same firing using a carbon die with 10 holes of the same diameter. The sintering conditions used are listed in Table 1. To evaluate the degree of sintering by SPS, part of the compacts were annealed at 1000°C for 24 h in a furnace (HIT-2300SG: Tokyo Vacuum Co., Kanagawa, Japan) evacuated of 10^{-3} Pa.

Table 1
Firing conditions of Ti powders by SPS. The compacts were 5 mm in diameter and 10 mm thickness

Sintering temperature	Sintering time	Sintering pressure	Current density	Current voltage	Vacuum
570°C	10 min	25 MPa	750 A	2–3 V	3–4 Pa

2.2. Mechanical testing

The weights (0.1 mg in accuracy) and external forms of the compacts after sintering were measured, and the apparent porosity was calculated from Ti density (4.53 g/cm^3) and the apparent volume. The compressive elastic modulus, proof strength and ultimate strength of the compacts were measured using a universal testing machine (DDS-5000, Shimadzu, Kyoto, Japan). A strain rate of 8.3×10^{-4}/s (cross head speed of 0.5 mm/min) was used.

2.3. Chemical treatments and immersion in SBF [12–14]

Half of the compacts were subjected to chemical treatment with an aqueous alkaline solution with and without subsequent annealing. The compacts were ultrasonically washed in acetone and ethyl alcohol for 15 min and dried in a desiccator under reduced pressure for 24 h. The specimens were soaked in a 5 M aqueous NaOH solution at 60°C for 24 h. After the alkaline treatment, the specimens were washed with distilled water, and dried in a desiccator for 24 h. The alkali-treated compacts were then heated to 600°C in an electric furnace in ambient air for 1 h, and cooled to room temperature.

Commercially available pure (99.5%) Ti disks were used as reference, that is, the disks were polished with #800 SiC papers. The disks were also ultrasonically washed in acetone and ethyl alcohol for 15 min and dried in a desiccator under reduced pressure. The dimensions of the disks were 1.0 mm in thickness and 33 mm in diameter. Their weights prior to surface modification and after the chemical process were measured. The effects of chemical treatment on apatite precipitation through the specimens were evaluated. The specimens with and without chemical treatment were immersed in Hanks' solution without organic species at 37°C in a Teflon-sealed bottle for 2 and 4 weeks with the solutions changed every 3 days to maintain the concentration of the solutions after the chemical reactions between Ti and the solutions. The volume of the solution was 50 ml per bottle and each sample was immersed in the solution. The pH of the solution was adjusted to 7.4 immediately after precipitation using $NaHCO_3$ solution. The ion concentrations of the solution are as follows: Na^+, 1.42×10^{-1}; K^+, 5.81×10^{-3}; Mg^{2+}, 8.11×10^{-4}; Ca^{2+}, 1.26×10^{-3}; Cl^-, 1.45×10^{-1}; HPO_4^{2-}, 7.78×10^{-4}; SO_4^{2-}, 8.11×10^{-4}; and CO_3^{2-}, 4.17×10^{-3} mol/l. The electrolytic concentration and pH of this solution are close to those of blood or extra-cellular fluid. No precipitate was formed in the solution. After immersion for 2 and 4 weeks, the compacts were rinsed in distilled water, dried in a vacuum desiccator and weighed using a microbalance to 0.1 mg accuracy. Mass change per initial weight was calculated for the compacts. For the disks, mass change per unit surface area was determined. For the estimation of the amount of elution in the SBF, an immersion test on the samples in distilled water was performed under the same experimental conditions as those used for SBF. The morphology of the precipitates was observed by scanning electron microscopy (SEM).

3. Results

The porosity and compressive strength of the sintered specimens are shown in Table 2. All the specimens in each batch had almost equal porosities. The compressive strength of the specimens sintered

by SPS was almost 110 MPa, and slightly lower than that of human cortical bone (110–170 MPa) [26]. However, the sintered specimens with annealing had a sufficiently high strength as biomaterials for hard-tissue replacement. This result suggests that SPS did not induce complete formation of bonding layers between powders. The elastic modulus, which determines the mechanical biocompatibility between the tissue and implant material, was 7–9 GPa, and close to that of cortical bone (17–20 GPa) [26]; here, that of pure Ti is 105–110 GPa. The annealing used in this study did not directly affect the elastic modulus of the specimens, because porosity affects elastic modulus and is not markedly affected by heat treatment.

The mass changes of the sintered specimens after immersion in SBF for 2 and 4 weeks are shown in Table 3. Here, the values are the mass gain ratio of the specimen after immersion in SBF to the specimen before pre-chemical treatment and immersion test. A significant increase in mass was not detected for the samples without chemical pretreatment. The surface morphologies of the precipitated crystals on the sintered compacts with and without chemical pretreatment are shown in Fig. 1. It was clear that the mass change induced by immersion in SBF due to precipitates on the Ti powders. From previous works [13,14] using thin-film X-ray diffractometry (TF-XRD) and X-ray photoelectron spectroscopy (XPS), the particles of the precipitate were identified as calcium phosphate, viz., bone-like apatite. Other particles such as NaCl might have been precipitated on the surface of the Ti powders upon chemical pretreatment, but were not identified in this study. The recrystallization and grain growth of the Ti powders were observed as shown in Figs 1c and 1d. The constitution and thickness of the oxide films on the powders for both compacts with and without subsequent annealing were not examined in this study, but were clearly different from the powders appearance. Table 4 shows the mass changes of the surface modified Ti before and after immersion in SBF solution compared with those of the discs. The mass changes of the compacts were about one hundred times higher than those of the discs. The ratio of mass increase for the actual surface area is discussed below. Elusion from the compacts with chemical pretreatment in SBF was detected. The compacts with the same pretreatment were then immersed in distilled water, and mass change was measured as shown in Table 5. The amounts of mass change were detected to be about 0.3–0.4% and a significant difference in mass were not observed between the compacts with and

Table 2

Elastic moduli, proof strengths and ultimate strengths of compacts with and without annealing determined by compressive test

	Compact by SPS	Compact with annealing
Porosity (%)	28 ± 1	25 ± 2
Elastic modulus (GPa)	7.9 ± 0.7	10.7 ± 1.2
Proof strength (MPa)	112 ± 9	350 ± 19
Ultimate strength (MPa)	112 ± 9	588 ± 169

Mean $\pm$ s.d. ($n = 3$).

Table 3

Mass changes of compacts after immersion in SBF. Data is calculated from the mass increments after immersion in SBF divided the mass after sintering

		2 Weeks (%)	4 Weeks (%)
Compact by SPS	Non-treated	0.06 ± 0.02	-0.05 ± 0.03
	Chemical treatment	2.69 ± 0.03	2.56 ± 0.01
Compact with annealing	Non-treated	0.03 ± 0.01	0.04 ± 0.09
	Chemical treatment	1.40 ± 0.05	1.38 ± 0.07

Mean $\pm$ s.d. ($n = 3$).

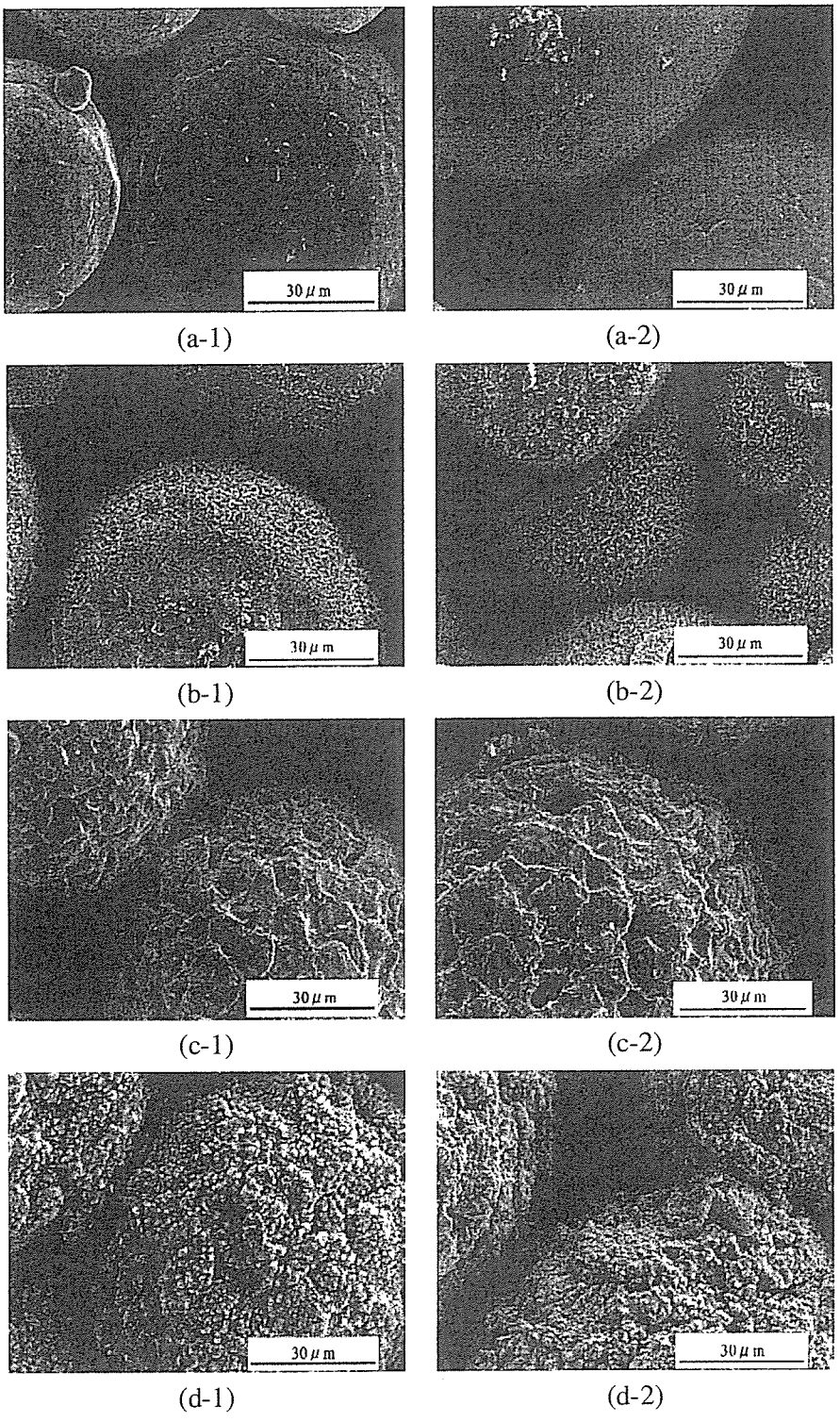

Fig. 1. Surface morphologies of precipitated apatite crystals on sintered compacts of Ti powders: (a-1) and (a-2) are sintered Ti compacts, that had been immersed in SBF for 2 and 4 weeks, respectively; (b-1) and (b-2) are the Ti compacts with chemical pretreatment, that had been immersed in SBF for 2 and 4 weeks respectively; (c-1) and (c-2) are the annealed Ti compacts, that had been immersed in SBF for 2 and 4 weeks, respectively; (d-1) and (d-2) are the annealed compacts with chemical pretreatment, which had been immersed in SBF for 2 and 4 weeks, respectively.

Table 4

Mass changes (mg) and mass change ratio per apparent surface area (mg/mm^2) of compacts. Here, the diameter and thickness of the disks and cylindrical compacts were 33 and 1.0 mm, and 5.0 and 9.7 mm (average), respectively

	Mass change (mg)		Mass change per apparent surface area (mg/mm^2)	
	2 Weeks	4 Weeks	2 Weeks	4 Weeks
Ti disc	0.7 ± 0.0	1.4 ± 0.1	4×10^{-4}	7×10^{-4}
Compact by SPS	16.6 ± 0.2	15.8 ± 0.0	9×10^{-2}	8×10^{-2}
Compact with annealing	8.8 ± 0.3	8.6 ± 0.4	5×10^{-2}	5×10^{-2}

Mean $\pm$ s.d. ($n = 3$).

Table 5

Mass changes of compacts with and without annealing induced by chemical treatment and immersion in distilled water for 2 and 4 weeks under the same conditions for immersion test in SBF

	Chemical pretreatment (%)	Immersion in SBF (%)		Immersion in distilled water (%)	
		2 Weeks	4 Weeks	2 Weeks	4 Weeks
Compact by SPS	1.95 ± 0.22	2.69 ± 0.03	2.56 ± 0.01	-0.32 ± 0.02	-0.36 ± 0.07
Compact with annealing	1.60 ± 0.03	1.40 ± 0.05	1.38 ± 0.07	-0.27 ± 0.00	-0.32 ± 0.01

Mean $\pm$ s.d. ($n = 3$).

without annealing. However, the chemical substances in the compacts were not identified in this study. Nonetheless, the mass change induced by pretreatment is not a negligible factor in the estimation of the amount of the precipitated apatite crystals.

4. Discussion

Increases in specific surface area, passive film thickness and crystal structure, chemical or electrochemical pretreatment of Ti oxides, and SBF composition are the factors for surface modification of Ti with calcium phosphates [27,28]. In this study, the effect of the specific area of a Ti specimen on the amount precipitated apatite crystals is confirmed. The relationship between the actual surface area of a Ti compact and diameter of a spherical particle is calculated as follows, if the junction area of the particles is not considered.

The specific ratio of the actual surface area to the apparent area, C, is represented as

$$C = \frac{p \cdot N}{S}.$$

Here, p is the surface area of each particle, i.e. $p = 4\pi(m/2)^2 = \pi m^2$, where m is the diameter of a particle. N is number of particles in the compact. S is the apparent surface area of the compact. The relationship between porosity, k, and the apparent volume of the compact, V, is

$$1 - k = \frac{\omega N}{V}.$$

Here, ω is the volume of a spherical particle, i.e. $\omega = 4\pi(m/2)^3/3 = \pi m^3/6$.

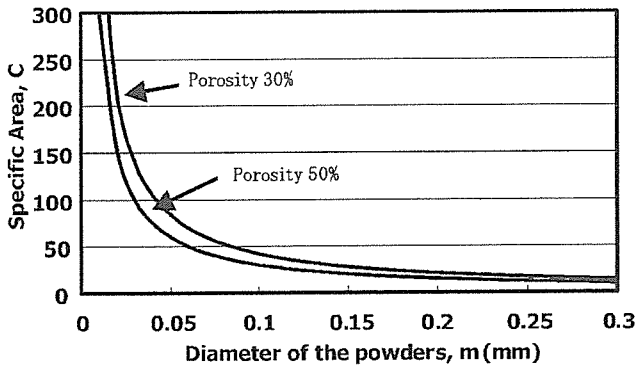

Fig. 2. Calculation results of relationship between diameter of powders and ratio of actual surface area to apparent surface area of cylindrical compact with diameter of 5 mm and height of 10 mm.

If the shape function is defined as the ratio of surface area to its volume, that for the spherical particle, f, is $f = p/\omega = 6/m$. The shape function, F, for a cylindrical compact can be represented as $F = 2(d + 2h)/hd$, where h and d are the height and diameter of a cylindrical compact. The specific ratio, C, is then

$$C = \frac{p}{\omega}\frac{V}{S}(1-k) = \frac{f}{F}(1-k) = \frac{3hd}{m(d+2h)}(1-k).$$

The relationship between the diameter of the particles and the specific ratio, C, for the porosity of 30% and 50% is graphically shown in Fig. 2. Here, the compact was 5 mm diameter and 10 mm height. As shown in this figure, diameter of the particle is effective factor in determining the specific ratio of C. Especially, C value is rapidly increased when the diameter of the powders is less than 100 μm. This result indicated that surface function of Ti is effectively reflected if the powders with the diameter of less than 100 μm are used for the compact.

The average diameter of the powders and the porosity of the compacts sintered in this study were 110 μm and 25–28%, respectively. The actual surface area of the specimen is then 40 times larger than that of the dense cylinder, that is, about 8000 mm^2 for the compact used. The mass changes (mg) per unit area (mm^2) for the immersion of 2 and 4 weeks were calculated to be 2.1×10^{-3} and 2.0×10^{-3}, and 1.1×10^{-3} and 1.1×10^{-3} mg/mm^2 for the compacts with and without annealing, respectively. These values for the specimens by SPS are about 3 times larger than that of the Ti discs (7×10^{-4} mg/mm^2), which was immersed in SBF for 4 weeks. Figure 3 shows a high-magnification image of the specimen with chemical pretreatment and subsequent immersion in SBF. The bridging of the precipitated particles between the Ti powders was clearly identified. This may be the reason for the large mass changes, which led to the precipitation of apatite crystals not only on the surface of Ti but also in the pores. If functional proteins or drugs are immobilized on metal implants, porous material modified by apatite crystals is helpful because many apatite particles with protein/drugs can be immobilized.

The heat treatment of the compacts affected the activity of the reaction in NaOH solutions. Different mass changes in SBF immersion were also detected, as shown in Tables 3–5. Low sintering temperatures 550–600°C used in SPS allows the deposition of passive surface films to rutile TiO_2. This rutile crystal can increase the surface energy and percentages of surface hydroxyl groups on Ti when it is immersed in a supersaturated calcium phosphate solution. Thus, it confers bioactivity on Ti [27]. However, subsequent annealing in a high-vacuum environment at 1000°C generates thin surface films on sintered Ti

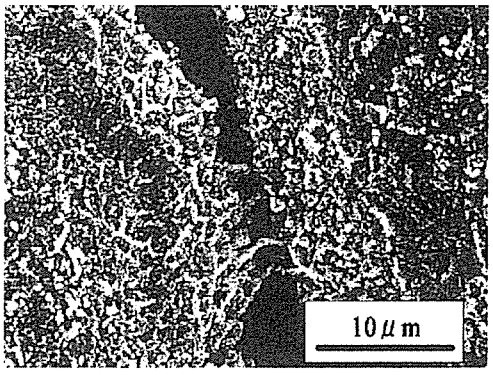

Fig. 3. Bridging feature of precipitated apatite crystals at bonding area of powders for sample, which had been chemically treated and subsequently immersed in SBF for 4 weeks.

powders. This may be the reason the mass changes showed different values between the compacts with and without annealing in a high-vacuum environment. It was concluded that control of crystal structure and the thickness of passive films are dominant factors governing surface modification with apatite by SBF immersion.

5. Conclusions

Because surface modification of a Ti depends on its surface oxide films, the increase of specific surface area on Ti using a porous structure was stimulated of precipitation of apatite in SBF. From the theoretical calculations, specific surface area is rapidly increased when the powders with less than 100 μm is used. Porous compacts with both biological and biomechanical compatibilities and high strength were developed since spherical powders of pure Ti with 110 μm diameter were sintered by SPS. Because apatite could adsorb proteins and/or drugs such as antibiotics, it is expected that a large amount of proteins and/or drugs could be impregnated when the porous compacts developed here are used.

References

[1] R. Van Noort, Titanium: the implant material of today, *J. Mat. Sci.* **22** (1987), 3801–3811.
[2] ASM, Heat treating of titanium and titanium alloys. in: *Metals Handbook*, 9th edn, American Society for Metals, OH, 1981, pp. 763–774.
[3] D. Scharnweber, R. Beutner, S. Rößler and H. Worch, Electrochemical behavior of titanium-based materials-are there relations to biocompatibility?, *J. Mat. Sci. Mater. Med.* **13** (2002), 1215–1220.
[4] D.F. Williams, Biocompatibility: An overview, in: *Concise Encyclopedia of Medical & Dental Materials*, D.F. Williams, ed., Pergamon Press, Oxford, 1990, pp. 51–59.
[5] K. De Groot, R. Geesink, C.P.A.T. Klein and P. Serekian, Plasma sprayed coatings of hydroxylapatite, *J. Biomed. Mater. Res.* **21** (1987), 1375–1381.
[6] L.H. Li, Y.M. Kong, H.W. Kim, Y.W. Kim, H.E. Kim, S.J. Heo and J.K. Koak, Improved biological performance of Ti implants due to surface modification by micro-arc oxidation, *Biomaterials* **25** (2004), 2867–2875.
[7] D. Ferro, S.M. Barinov, J.V. Rau, R. Teghil and A. Latini, Calcium phosphate and fluorinated calcium phosphate coatings on titanium deposited by Nd:YAG laser at a high fluence, *Biomaterials* **26** (2005), 805–812.
[8] H. Ishizawa and M. Ogino, Formation and characterization of anodic titanium oxide films containing Ca and P, *J. Biomed. Mater. Res.* **29** (1995), 65–72.
[9] B. Yang, M. Uchida, H.M. Kim, X. Zhang and T. Kokubo, Preparation of bioactive titanium metal via anodic oxidation treatment, *Biomaterials* **25** (2004), 1003–1010.

[10] P.A. Ramires, A. Wennerberg, C.B. Johansson, F. Cosentino, S. Tundo and E. Milella, Biological behavior of sol-gel coated dental implants, *J. Mat. Sci. Mater. Med.* **14** (2003), 539–545.
[11] H.Q. Nguyen, D.A. Deporter, R.M. Pilliar, N. Valiquette and R. Yakubovich, The effect of sol-gel-formed calcium phosphate coatings on bone ingrowth and osteoconductivity of porous-surfaced Ti alloy implants, *Biomaterials* **25** (2004), 865–876.
[12] H.M. Kim, F. Miyaji, T. Kokubo and T. Nakamura, Preparation of bioactive Ti and its alloys via simple chemical surface treatment, *J. Biomed. Mater. Res.* **32** (1996), 409–417.
[13] T. Hanawa, M. Kon, H. Ukai, K. Murakami, Y. Miyamoto and K. Asaoka, Surface modification of titanium in calcium-ion-containing solutions, *J. Biomed. Mater. Res.* **34** (1997), 273–278.
[14] K. Hamada, M. Kon, T. Hanawa, K. Yokoyama, Y. Miyamoto and K. Asaoka, Hydrothermal modification of titanium surface in calcium solutions, *Biomaterials* **23** (2002), 2265–2272.
[15] F. Barrere, C.A. van Blitterswijk, K. de Groot and P. Layrolle, Nucleation of biomimetic Ca–P coatings on Ti6Al4V from a SBF × 5 solution: influence of magnesium, *Biomaterials* **23** (2002), 2211–2220.
[16] S.R. Frenkel, J. Simon, H. Alexander, M. Dennis and J.L. Ricci, Osseointegration on metallic implant surfaces: effects of microgeometry and growth factor treatment, *J. Biomed. Mater. Res. (Appl. Biometer.)* **63** (2002), 706–713.
[17] Y. Liu, E.B. Hunziker, N.X. Randall, K. de Groot and P. Layrolle, Proteins incorporated into biomimetically prepared calcium phosphate coatings modulate their mechanical strength and dissolution rate, *Biomaterials* **24** (2003), 65–70.
[18] S. Hanada, T. Ozaki, E. Takahashi, S. Watanabe, K. Yoshimi and T. Abumiya, Composition dependence of Young's modulus in beta titanium binary alloys, *Mater. Sci. Forum.* **426–432** (2003), 3103–3108.
[19] K. Asaoka and N. Kuwayama, Mechanical properties and biomechanical compatibility of porous titanium for dental implants, *J. Biomed. Mater. Res.* **19** (1985), 699–713.
[20] S. Thelen, F. Barthelet and L.C. Brinson, Mechanics considerations for microporous titanium as an orthopedic implant material, *J. Biomed. Mater. Res.* **69A** (2004), 601–610.
[21] A.I. Itälä, H.O. Ylänen, C. Ekholm, K.H. Karlsson and H.T. Aro, Pore diameter of more than 100 μm is not requisite for bone ingrowth in rabbits, *J. Biomed. Mater. Res. (Appl. Biomater.)* **58** (2001), 679–683.
[22] D.C. Dunand, Processing of titanium foams, *Adv. Eng. Mater.* **6** (2004), 369–376.
[23] H. Guo, K.A. Khor, Y.C. Boey and X. Miao, Laminated and functionally graded hydroxyapatite/yttria stabilized tetragonal zirconia composites fabricated by spark plasma sintering, *Biomaterials* **24** (2003), 667–675.
[24] M. Kon, L.M. Hirakata and K. Asaoka, Porouse Ti–6Al–4V alloy fabricated by spark plasma sintering for biomimetic surface modification, *J. Biomed. Mater. Res. (Appl. Biomater.)* **68B** (2004), 88–93.
[25] L.G. Yu, K.A. Khor, H. Li and P. Cheang, Effect of spark plasma sintering on the microstructure and in vitro behavior of plasma sprayed HA coatings, *Biomaterials* **24** (2003), 2695–2705.
[26] W.G. Billotte, Ceramic biomaterials, in: *The Biomedical Engineering Handbook*, J.D. Bronzino, ed., 2nd edn, CRC Press LLC, FL, 2000, pp. 38–111.
[27] B. Feng, J.Y. Chen, S.K. Qi, L. He, J.Z. Zhao and X.D. Zhang, Characterization of surface oxide films on titanium and bioactivity, *J. Mater. Sci. Mater. Med.* **13** (2002), 457–464.
[28] Y.T. Sul, C.B. Johansson, S. Petronis, A. Krozer, Y. Jeong, A. Wennerberg and T. Albrektsson, Characteristics of the surface oxides on turned and electrochemically oxidized pure titanium implants up to dielectric breakdown: the oxide thickness, micropore configurations, surface roughness, crystal structure and chemical composition, *Biomaterials* **23** (2002), 491–501.

Materials Science Forum Vols. 539-543 (2007) pp. 3649-3654
online at http://www.scientific.net
© (2007) Trans Tech Publications, Switzerland

Effect of Surface Oxide Films on Degradation of Titanium

Kenzo Asaoka[1, a] and Kunimitsu Maejima[2, b]

[1]Department of Biomaterials and Bioengineering, Institute of Health Biosciences,
The University of Tokushima
3-18-15 Kuramoto-cho, Tokushima, 770-8504, Japan
[2]ESCO, ltd.
1-3-12 Nishikubo Musashino-shi, Tokyo 180-0013, Japan
[a]asaoka@dent.tokushima-u.ac.jp, [b]maejima@escoltd.co.jp

Keywords: Titanium, Corrosion, Mass spectrometry, Hydrogen, Titanium hydride, Oxidation.

Abstract. Thermal desorption spectroscopy (TDS) was applied to measure the hydrogen in titanium (Ti). Because fracture by hydrogen embrittlement for medical/dental devices of Ti and Ti alloys was reported, dependence of surface oxidation film on hydrogen absorption and desorption behaviors of cp-Ti was carried out. To form the surface oxide film (rutile), the Ti wire samples were annealed in an ambient air at 800°C for 2 hours. Half of the specimens were immersed in a mixed solution of NaF and H_3PO_4 (APF). The part of the specimens were removed the surface films by abrasion after the heat and the immersion in the APF solution. TDS analysis was applied to detect released ions/molecules during heating from room temperature to 1200°C in a high vacuum vessel for the TiH_2 powders, the Ti samples with and without the above treatments. High ion intensity was detected for hydrogen (m/z = 2), and ion intensities of the other ions/molecules were almost the background level in measurements. The concentration of hydrogen in the samples related with heat and chemical process was determined quantitatively, and was not significantly increased by the annealing and the immersion in APF solution if the sample had the tough surface film. However, the sample, which had been removed the surface films before the immersion in APF, showed typical chemical degradation after the immersion in APF for 7 days, that is, high ion intensities of hydrogen, fluoride, water and hydroxyl ions were detected. It was concluded that the control of the surface oxide film on the medical/dental Ti devices is important in determining its longevity.

Introduction

Titanium (Ti) is an active metal. However, surface oxide film (TiO_2) provides corrosion resistance and biocompatibility to the metal. The surface of Ti, which had been working and/or polishing/grinding, has non-crystal thin oxide film, and corrosion resistance of the Ti is not sufficient. When the Ti is annealed in an ambient air, the metal is covered with the crystalline oxide films such as anatase and rutile, and is improved its corrosion resistance. However, thickness of the oxide film becomes rapidly increase at high temperature than 1000°C, and flakes fall down as a scale. It is recognized that the control of the surface film on Ti is essentially important for use as corrosion-resistant alloy [1]. Mechanism of bio-compatibility of Ti for bone tissue is recognized as follows: When the Ti immerse in body fluid, a fine hydroxyapatite (calcium phosphate) crystals are formed to coalesce into the oxide film. The precipitated crystals are connected with bone cells directly, because apatite is a main component of the bone structure. The amount and the rate of the precipitation reaction of apatite on the Ti substrate are depended on the crystal structure of the oxide film of the Ti [2]. From an electro-chemical study, corrosion mechanism of metal is carried out using corrosion diagrams by Pourbaix [3]. In thermodynamically stable region in water at 1 atm (1 x 10^5 Pa), Ti is passive state. However, it is known that the Ti is deteriorated in solutions containing fluoride ions.

All rights reserved. No part of contents of this paper may be reproduced or transmitted in any form or by any means without the written permission of the publisher: Trans Tech Publications Ltd, Switzerland, www.ttp.net. (ID: 150.59.88.229-26/12/06,08:13:10)

Thermal desorption spectroscopy (TDS) is a method to analyze released ions by quadrupole mass spectrometer (QMS) during heating sample in a high vacuum vessel. This is a helpful method to take information for the adsorbed and/or uptake ions to the specimen. In this research, release ions/molecules from the Ti hydride (TiH_2) powders, cp-Ti wires, the annealed cp-Ti wires and the cp-Ti wires, which had been immersed in APF solution, were analyzed by TDS. Effects of the annealing and the immersion treatment in APF solution on uptake and/or absorbed ions/ molecules were determined. Relationship between the surface oxide films and degradation of the Ti substrate were discussed.

Materials and Method

Ti-hydride (TiH_2) powders with grain size of 150 μm under (Sumitomo Titanium Co., Amagasaki, Japan), commercial available pure (> 99.5%) titanium wires with a diameter of 0.6 mm (TI-451414: Nilaco Co., Tokyo, Japan) were used as materials for experiment. As-received wires were polished with #800 SiC papers. The wires were then ultrasonically washed in acetone and distilled water for 15 min. The specimens were annealed at 800°C for 2 h in an ambient air by an electrical furnace. A part of the annealed specimens were immersed in aqueous solution of 2.0% acidulated phosphate fluoride (APF; 2.0% NaF +1.7% H_3PO_4) with pH 5.0 at 37°C. The specimens, which had been removed the surface oxide films by abrasive papers, were ultrasonically washed. The surface morphology of each specimen was observed by scanning electro microscope (SEM). Released ions from the TiH_2 powders and the Ti wire samples in a high vacuum chamber (1.3×10^{-7} Pa) were measured by TDS (EMD-WA1000S/W: ESCO, Tokyo) during heating of 0.17°C/s and 0.5°C/s, respectively. Time interval of detection of the released ions by QMS was 4 s and 5 s for the TiH_2 powders and the Ti wire specimens, respectively. Table 1 shows list of the heat and the immersion treatments of the Ti wire samples measured in this study with symbol codes.

Table 1 Ti wire samples analyzed by TDS

Code	Treatments
A	No treatment: reference sample
B-1	Heated at 800°C for 2 h
B-2	Removed surface films by abrasion for B-1
C-1	Immersed in APF solution for 30 days for B-1
C-2	Removed surface films by abrasion for C-1
C-3	Immersed in APF solution for 7 days for B-2

Quantitative analysis of hydrogen

Silicon (Si) plate, in which hydrogen ions had been implanted, is used for a standard material to quantitative analysis of hydrogen, because hydrogen in the Si plate is stable at room temperature and most of hydrogen in it is released during heating process in high vacuum vessel. Ion intensity data of hydrogen for the Si plate ($10 \times 10 \times 0.62$ mm^3), which had been implanted 1×10^6 hydrogen ions, is measured by TDS. Then, number of released hydrogen molecules (H_2) from the standard material should be 5×10^{15}. Integrated value of the ion intensity curve for hydrogen on temperature can be a reference data for the samples for quantitative analysis of hydrogen in the samples. Amount of released hydrogen from the sample is calculated from integrated value of the ion intensity curve during heating under the same experimental conditions as that of the reference data. The concentration of hydrogen in the sample, C (mass %), can be calculated using an equation of $C = MNA_0/W$, when all of the hydrogen in the material is released during heating. Here, M is the atomic mass unit of hydrogen molecule (2 g), A_0 is Avogadro's number (6.02×10^{23} amu/g), W is the mass of the sample. N is the number of the released hydrogen molecules from the sample. Here, the ion intensity for m/z = 2 (m/z is a ratio of mass to electronic charge) is a typical index for the detection of hydrogen.

Results

Titanium hydride powders

The TDS fragments of each m/z for the released ions/molecules from the TiH_2 powders during heating are shown in Figure 1. Here, vertical axis is represented ion-intensity (A) for each m/z fragment. Figure 2 shows fragments of 2nd run of the same sample, that is, after heating of the 1st run to 1200°C, the sample was cooled down to room temperature in a high vacuum vessel, and the sample was reheated under the same experimental conditions for the TDS analysis. A peak of high ion intensity for m/z = 2 was clearly identified at ca. 600°C. Low peak of the fragment for m/z=18, that is the fragment related with water, was detected. However, the other ion intensities were low and almost background level in the detection. For the 2nd run, each of the ion intensities was low and within background level. It was suggested that any molecules/ions were not released from the powders during the 2nd run. Hydrogen in the powders had been fully released during the 1st run. For quantitative analysis of hydrogen, the ion intensity for m/z = 2 in Fig. 1 is modified and drawn in Figure 3. The amount of released hydrogen during 1st run was calculated to be 2.94 mass% (59.0 at%) from the quantitative analysis. The data was well agreed with amount of hydrogen in Ti hydride (TiH_2). These results suggested that Ti hydride was decomposed to Ti and hydrogen during heating of the 1st run.

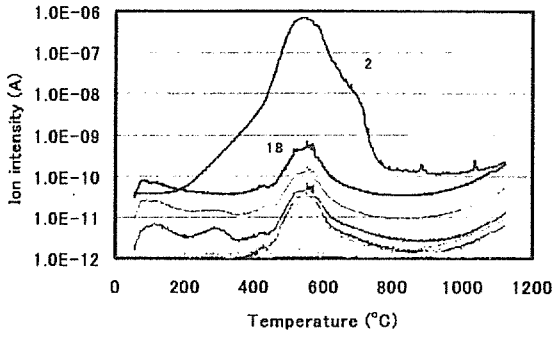

Figure 1 Ion intensity curves of the released ions/molecules from the TiH_2 powders by TDS analysis.

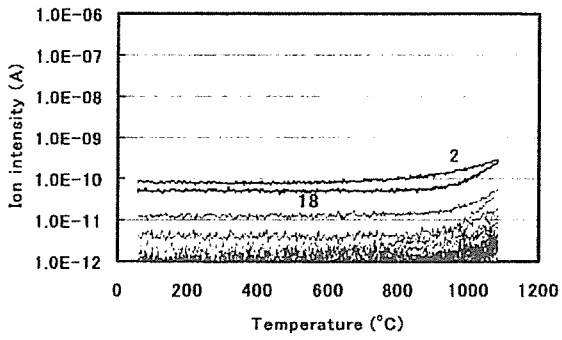

Figure 2 Ion intensity curves for the TiH_2 powders, which had been fired once in a high vacuum vessel (2nd run).

As-received Ti sample (A)

The surface morphology of the sample A (as-received cp-Ti wire) could observe scratches, which might be caused by drawing through die, along longitudinal direction. From high magnification photographs, tear cracks were observed. The sample A was heated to 1200°C (1st Run), and cool down to room temperature in the evacuated chamber in the TDS equipment. After that, the sample A was reheated to 1200°C (2nd Run). Figure 4 shows net ion intensity of hydrogen (m/z = 2), which was released from the sample A, that is, the data is subtracting the background (2nd run) from the data of the 1st run. Integrated value of ion intensity curve from room temperature to 1000°C, was compared with the reference data, and 1.1 x 10^{17} for 10 mg was calculated for number of the released hydrogen molecules from the sample A. From this value, concentration of hydrogen in the sample A was calculated to be 37 mass ppm (ppm is mass ppm for the following expression).

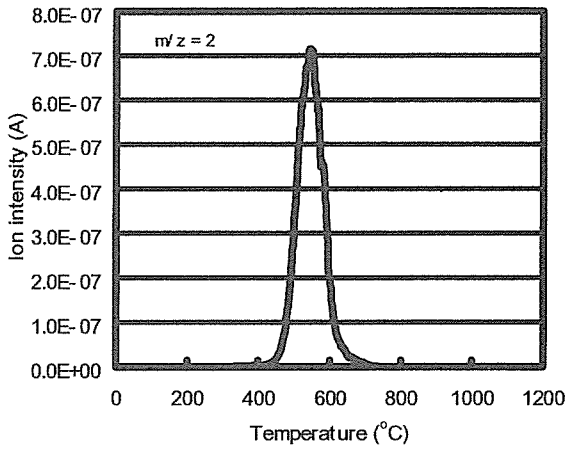

Figure 3 Ion intensity curve of the m/z = 2 (hydrogen) for the TiH_2 powders.

Annealed sample (B-1 and B-2)

The surface morphology of the annealed sample B-1 was similar to that of the sample A from the SEM photos. However, surface thick oxide films were confirmed from visual inspection. By annealing at 800°C, the oxide films might be formed rutile and a few μm in thickness. Designation of B-2 is the sample, which have been removed its oxide films from the sample B-1 by abrasion. Figure 5 shows the ion intensity for m/z = 2 for the specimens B-1 and B-2 compared with the reference sample A. For the sample B-1, TDS measurements were repeated 4 times in the evacuated chamber, because the oxide films protect release of hydrogen in the Ti. Detected ion intensity of hydrogen (m/z = 2) was decreased according to the heating cycles. On the contrary, curve with peak intensity was detected for the sample B-2, which was the similar curve with the sample A. Onset temperatures at release of hydrogen were almost same for the samples measured. These results indicated that diffusion rate of hydrogen through the surface the oxide films is low, that is, the oxide film play an important role on protect of occlusion and dislodgement of hydrogen. The amount of hydrogen was calculated to be 33 ppm and 40 ppm (total of 4 times heating) for the B-1 and B-2, respectively, and almost equal to the amount of that of the reference sample A. It was concluded that the Ti did not uptake the hydrogen significantly during the annealing.

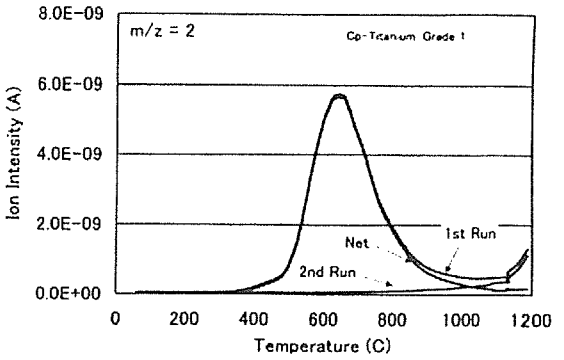

Figure 4 Ion intensity curve of the m/z = 2 for the as-received cp-Ti wire sample.

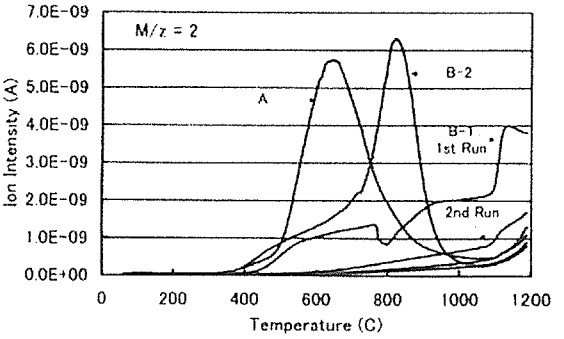

Figure 5 Ion intensity curves of the m/z = 2 for the annealed cp-Ti wire samples with and without surface oxide film.

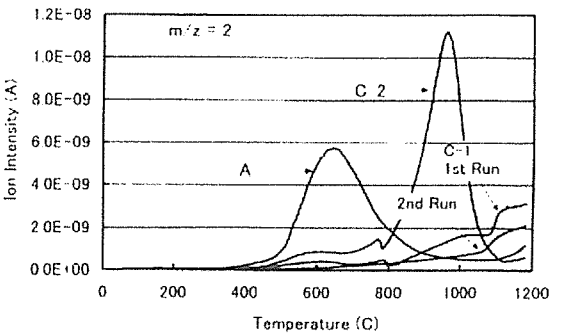

Figure 6 Ion intensity curves of the m/z = 2 for the cp-Ti wire samples, which had been immersed in APF solution, after anneal heat treatment in an ambient air. C-1 and C-2 are the samples with and without surface oxide at TDS analysis.

Immersed in APF solution (C-1, C-2, and C-3)

Surface of the specimen C-1, which was annealed and immersed in APF, was almost the same feature as that of the specimen B-1, that is, traces of typical chemical attack was not observed. Figure 6 shows results of the TDS analysis, that is, the curves of m/z = 2 for the samples of C-1 and C-2 are shown in comparing with that of the sample A. The curve of the sample C-1, which was covered with the oxide films, was the curve with increasing the ion intensity as the increasing temperature. Decreasing of the ion intensity was observed for the 2nd run. The m/z = 2 curve of the sample C-2, which was removed the oxide films after the immersion in APF solution, shows peak similar to tht of the samples A and B-2. However, the peak temperature is higher than that of the other specimens. Amount of hydrogen, which was released from the sample of 10 mg, was calculated to be 26 and 47 ppm for the specimen C-1 and C-2, respectively. This results show the significant

increase of hydrogen intake for the Ti specimens with the oxide films, which had been formed by the annealing, was not detected by the immersion in APF solution. Surface of the specimen C-3, which had been removed the surface films after the annealing and the immersed in APF for 7 days was drastically attacked by the solution, and pores were observed on the surface. Figure 7 shows the ion intensities curves by the TDS for the specimens of C-3. SEM photos and the results of ion intensity curves by the TDS showed that the specimen C-3 had a severe chemical attack from the solution. Not only hydrogen and water but also fluoride and sodium ions, which were the components of APF solution, were detected in high intensities. The m/z = 17 and 18, which were related with ions of water molecules, were high at lower temperature than 400°C, and at the higher temperature than 400°C, that of hydrogen (m/z = 2) was extremely high. Amount of hydrogen was calculated to be 864 ppm, and the value was twenty times higher than the specimens with the oxide films by the annealing. Peak of ion intensity related with fluorine (m/z = 20 (HF) and 19 (F)) were detected in the range of 10^{-9} A order intensity. The amount of detected hydrogen for the Ti specimens was summarized and listed in Table 2.

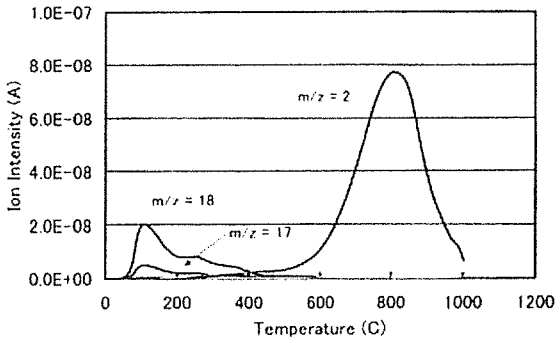

Figure 7 Ion intensity curves of the m/z = 2 for the cp-Ti wire samples, which had been removed the surface oxide films and immersed in APF solution, after anneal heat treatment in an ambient air.

Table 2 Hydrogen concentrations in the Ti samples with various treatments.

Symbol	Number of Hydrogen/10 [mg]	[ppm]
A	1.1×10^{17}	37
B-1	9.8×10^{16}	33
B-2	1.2×10^{17}	40
C-1	7.9×10^{16}	26
C-2	1.4×10^{17}	47
C-3	2.6×10^{18}	864

Discussion

TDS fragment curves

According to phase diagram [4], Ti-H system is a eutectoid type. Maximum solubility of H in α-Ti is 7.9 at % at the eutectoid temperature and 40 - 50 ppm at room temperature. Dissolved hydrogen as interstitial atoms and hydrogen in precipitate hydrides are the atoms to release from the α-Ti substrate. When Ti was heated in a high vacuum vessel, desorption of hydrogen starts from ca. 200°C, and decomposition of hydride become active at higher temperature than that. This experimental result wass agreed with the phase diagram, that is, onset of hydrogen detection is ca. 300°C. The amount of detected hydrogen is determined from diffusion rate of hydrogen in Ti and decomposition rate of hydrides. Diffusion and phase decomposition rate are theoretically represented by Arrhenius equation ($D = D_0 \exp(-Q/RT)$). The equation suggested that the amount of detected hydrogen increase with increasing temperature. If the diffusion rate is high, the ion intensity curve of the hydrogen is increased abruptly. Thermal instability, distribution and size of the precipitates (TiH_2) affect directly to the ion intensity fragment curve. At higher temperature, decomposition of hydrides is accelerated, and the size of hydride is decreased, that is, the released hydrogen is decreased. This assumption is well agreed with the experimental data.

From comparison of the DTS curves for the as-received sample (A), the annealed sample without the surface films (B-2), and the sample after the immersion in APF and removed the surface films (C-2), amount of the hydrogen and onset temperature are almost the same to each other. However, the peak temperature for the sample A is ca. 600°C. That of the sample B-2 and C-2 are shifted to higher temperature. Because diffusion rate is high for the matrix with working structure and fine distributed hydrides, low peak temperature showed for the sample A. Growth of

precipitated hydrides and stabilization of the hydride during the annealing at 800°C, might be resulted for the higher peak temperature of desorption. Peak was also shift to high temperature by the immersion in APF solution. The intake hydrogen is low during the immersion in SBF solution, because of shielding effects of hydrogen. However, results suggested that the intake hydrogen, that is low but not negligible, affect to make thermally stable in α-Ti.

Hydrogen embrittlement

Hydrogen, oxygen, nitrogen and carbon are known as interstitial impurity atoms in Ti, and they increase strength of Ti by solid solution hardening, except for hydrogen. Titanium, which contains higher than 100-200 ppm hydrogen, is lost its ductility and increase notch sensitivity. This phenomenon is known as hydrogen embrittlement. From this, solubility of hydrogen in cp-Ti, which is used for implant materials, is standardized as follows: the hydrogen contents is lower than 100, 125, and 150 ppm for small billet, bar and billet, and flat products, respectively. Titanium oxide layer, which is a few nano meter in thickness, are automatically generated when the metal surface is exposed to an ambient air by cutting and/or grinding. This oxide layer exerts a protective action, and Ti posses a high corrosion resistance. However, this corrosion resistance is not adequate to use in a severe corrosive environment such as in vivo. From the TDS curves for hydrogen of the specimen with oxide films, diffusion rate of hydrogen through the titanium oxides is extremely low. The surface film traps the release of hydrogen. Titanium oxide (rutile) plays an important role to protect the hydrogen uptake in vivo and an ambient environment. The results of the immersion in the APF solution of the specimen C-3 shows that amount of hydrogen uptake is 20 times compare with initial concentration during 7 day's immersion. Because Ti is an active metal, water, fluoride and sodium ions were detected from the specimen C-3. Hydrogen content, which is absorbed during working and cleaning, is most serious problem for use of Ti. However, hydrogen content in Ti is increased in biological structures using for medical device. For example, hydrogen embrittlement of super-elastic Ni-Ti orthodontic wire and titanium dental implant were reported [5]. Reason of the fracture is inferred that insufficient thickness of the oxide film allows the hydrogen uptake in the mouse. Thus, it is important that the formation of the oxide films such as rutile and anatase, is elongate the longevity of the medical and dental devices.

Conclusion

Ti hydride powders, as-received cp-Ti samples, the annealed cp-Ti samples and the annealed samples with the immersion in APF solution were analyzed by TDS, and measured effect of the oxide films on degradation of Ti. From these experimental results, hydrogen was the main released ions/molecules from the samples. Water and hydroxyl ion were also detected. The concentration of hydrogen in the Ti sample was not increased significantly by the annealing at 800°C and the immersion in SBF solution. However, degradation of the Ti sample was measured for the samples without the surface films (removed the oxide film by abrading), and hydrogen, fluoride, water and hydroxyl ions were detected. It was concluded that the control of the surface oxide film is important to use Ti devices.

References

[1] ASM: *Metals Handbook Vol. 4: Heat Treating* (ASM 1981).

[2] T. Albrektsson: *Critical Reviews in Biocompatibility I* (CRC Press 1985)

[3] M. Pourbaix: *Atlas of electrochemical equilibria in aqueous solutions* (National Association of Corrosion Engineers 1974)

[4] M. Hansen: *Constitution of binary alloys* (McGraw-Hill 1968)

[5] K. Asaoka et al: Met. Mater. Trans. A Vol.33A(2002), p.495.

厚生労働科学研究費補助金

化学物質リスク研究事業

ナノ微粒子の体内動態可視化法の開発

（課題番号 ： H18-化学--一般-006）

平成 18 年度春季
第 1 回目標策定研究発表会

日時：平成 18 年 5 月 17 日～18 日

場所：支笏湖「丸駒温泉旅館」

平成18年度研究組織

［主任研究者］

亘理 文夫　　北海道大学大学院歯学研究科　口腔健康科学講座　教授

［分担研究者］

田路 和幸　　東北大学大学院環境科学研究科　教授
戸塚 靖則　　北海道大学大学院歯学研究科　口腔病態学講座　教授
横山 敦朗　　北海道大学大学院歯学研究科　口腔機能学講座　教授
北川 善政　　北海道大学大学院歯学研究科　口腔病態学講座　教授
森田　学　　北海道大学大学院歯学研究科　口腔健康科学講座　教授
朝倉 清高　　北海道大学触媒科学研究センター　教授
古月 文志　　北海道大学大学院地球環境科学院　教授
大貫 惣明　　北海道大学大学院工学研究科　教授
遠山 晴一　　北海道大学大学院医学研究科　助教授
石川 邦夫　　九州大学大学院歯学研究科　教授
岡崎 正之　　広島大学大学院医歯薬学総合研究科　教授
浅岡 憲三　　徳島大学ヘルスバイオサイエンス研究部　教授

［研究協力者（順不同）］

市野瀬 英喜　　北海道大学エネルギー先端工学研究センター（超高圧電子顕微鏡）教授
大森 守　　東北大学　エネルギー安全科学国際研究センター　研究支援者
鈴木 邦明　　北海道大学大学院歯学研究科　口腔病態学講座　教授
市原 学　　名古屋大学大学院医学系研究科　健康社会医学専攻　社会生命科学講座
矢田 慶治　　東北大学　名誉教授
奥山 文雄　　名古屋工業大学　名誉教授
久保木 芳徳　　北海道大学　名誉教授
宇尾 基弘　　北海道大学大学院歯学研究科　口腔健康科学講座　助教授
赤坂 司　　北海道大学大学院歯学研究科　口腔健康科学講座　助手
佐藤 義倫　　東北大学大学院環境科学研究科　助手
高師 則行　　北海道大学大学院歯学研究科　口腔病態学講座　助手
田村 一央　　北海道大学大学院歯学研究科　口腔病態学講座　非常勤助手
野田坂佳伸　　北海道大学大学院歯学研究科　中央研究部　助手
青木 尚史　　北海道大学大学院歯学研究科　口腔機能学講座　大学院生
阿部 薫明　　北海道大学大学院先端生命科学研究院　学術研究員
岡崎 良子　　名古屋工業大学大学院工学研究科　しくみ領域産学官連携研究員
王 蔚　　北海道大学大学院理学研究科　高分子材料解析学　COE研究員
朱 禹赫　　北海道大学大学院歯学研究科　口腔健康科学講座　大学院生
越川 高光　　北海道大学大学院歯学研究科　口腔健康科学講座　大学院生